Heat and Mass Transfer (2023) 59:1635–1646
https://doi.org/10.1007/s00231-023-03356-w

ORIGINAL ARTICLE

Experimental investigation of a novel heat exchanger for optimizing heat transfer performance using Al_2O_3-water nanofluids

S. Hamidatou[1,5] · M. Nadir[1] · Hussein Togun[2] · Azher M. Abed[3] · K. Deghoum[4] · A. Hadjad · Goodarz Ahmadi[6]

Received: 26 August 2022 / Accepted: 7 March 2023 / Published online: 30 March 2023

Abstract

This study presents an experimental investigation to determine the heat transfer enhancement in a novel heat exchanger known as the "Helicoidal Square-Shaped Heat Exchanger" with and without using a nanofluid. The experiments were performed for the range of Reynolds numbers from 4400 to 8000, using nanofluid (Al_2O_3-pure water) at the concentrations 0.1, 0.25, and 0.5%. This experimental investigation found that the heat transfer ratio is improved by increasing the nanofluid concentrations and the flow Reynolds number. The highest value of the heat transfer ratio was at Re = 8000, and 0.5% concentration of nanofluids. The corresponding increment in the heat transfer rate was 13.46 %, the heat transfer coefficient augmented by 9.64 %, and the Nusselt number improved by 10.43% compared to the results obtained experimentally with distilled water. The results obtained for the distilled water were verified with the Dittus-Boelter equation and numerical simulation. In addition, all obtained experimental data were compared with the CFD simulation. The use of nanofluids for heat transfer enhancement has a wide range of applications. Therefore, the presented results suggest using Al_2O_3-water nanofluids to improve the efficiency of many renewable energy plants, including solar and geothermal energy systems.

Nomenclature

Symbols

S	Area of heat transfer (m2)
k	Thermal conductivity (W/m /K)
h	Heat. Transfer. coefficient (W/m2/K)
η	Heat transfer enhancement
T	Temperature (^oC)
∅	Volume concentration (%)
ω	Weight concentration wt (%)
ρ	Density of nanoparticles (kg/m3)
u	Dynamic. Viscosity (kg/ m.s)
φ	Volume. Fraction φ = ∅/100
T_r	Reference temperature in the tank (^oC)
C_p	Specific heat (J /kg /K)
Re	Reynolds number
Nu	Nusselt number
Pr	Prandtl number
D	Tube diameter(m)
$\dot{m}$	Masse flow (kg/s)
η_e	Effectiveness of heat transfer fluid
W_p	Pumping power consumption
$T_{(w,ave)}$	average temperature of the inner pipe surface
$T_{(b,ave)}$	average temperature of the fluid inside the pipe
Q	Heat flux (W)

Subscripts

p	Particles
bf	Base fluid
nf	Nanofluid
f	Fluid
r	Reference
in	Inlet
out	outlet

✉ S. Hamidatou
s.hamidatou@univ-boumerdes.dz

✉ Hussein Togun
htokan_2004@yahoo.com; hussein-tokan@utq.edu.iq

[1] Energy and Mechanical Engineering Laboratory (LEMI), University of Boumerdes, Boumerdes, Algeria

[2] Department of Biomedical Engineering, College of Engineering, University of Thi-Qar, Thi-Qar 6400, Iraq

[3] Air conditioning and Refrigeration Techniques Engineering Department, Al-Mustaqbal University College, Babylon 51001, Iraq

[4] Renewable Energy Development Unit in Arid Zones (UDERZA), University of El Oued, 39000, El Oued, Algeria

[5] Laboratory of New and Renewable Energy Development in Arid Zones (LENREZA), University of Ouargla, BP511 Ouargla, Algeria

[6] Department of Mechanical and Aerospace Engineering, Clarkson University, Potsdam, NY 13699-5725, USA

HE	Heat Exchanger
HSSHE	Helical Square Shape Heat Exchanger
PH	Potential hydrogen
IEP	Iso Electric Point
PEC	Performance efficiency coefficient
i	Step
a	Rib length
b	Hight

1 Introduction

Many researchers worldwide focus on finding solutions to enhance heat transfer with applications to the development of renewable energies (solar and geothermal) systems. Various techniques have been used to improve heat transfer in fluids. Some were motivated to improve heat transfer by creating different geometric shapes, while others used nanofluids [1]. Singh et al. [2] suggested modifying the heat exchangers' geometry as an important approach to improving heat transfer. Some studies adopted the same idea to improve the thermal performance by changing the rectangular wings, hollow circular discs into different shapes, warped cables [3], warped plates [4], conical rings [5], and vortex conical/rod strip generator [6]. Previous studies confirmed that using solid forms inside the tube enhances thermal performance by creating small vortices and changing the type of fluid flow to turbulence. On the other hand, nanofluids are an attractive alternative to simple base fluids due to their higher thermal conductivity and are the ideal heat transfer medium for heat exchangers [7]. Hassen et al. [8] examined the insertion of a new conic helical basket heat exchanger (CBHE). They suggested that their system could be used for greenhouse cooling. In addition, they used a system with two conic baskets serially connected and compared their thermal performance for horizontal and vertical orientations.

Many previous studies concerning nanoparticle use in heat transfer were reported in the literature. Kumar et al. [9] concluded that using nanofluid in heat transfer necessitated higher pumping capacity, increasing operation costs. Nacira et al. [10] studied a heat exchanger using copper oxide nanofluids to investigate the heat transfer rate. Their findings revealed that the heat transfer flux improved by 17.4 % and the heat transfer coefficient by 40 % when water-based nanofluids with the 2-vol% CuO nanoparticles were used. Wilk et al. [11] found that the increase in heat transfer flux is due to the higher thermal conductivity of nanofluids, even at a low concentration. Karuppsamy et al. [12] considered the influence of CuO nanofluid on the heat transfer in a cone-shaped heat exchanger tube; their work revealed that collision between nanoparticles and the insert wall results in the rising of the pressure drop along the tube.

Narei et al. [13] evaluated the impact of using nanofluid on reducing a vertical Heat Exchanger bore length and found that the nanofluid caused a 1.3% reduction in the necessary bore length. Jamshidi [14] conducted a numerical study on extracting heat energy from the helical fin heat exchanger, taking into account the effect of different nanoparticle diameters that showed an improvement in heat transfer and an increase in heat transfer coefficient. In an experimental study, Arani et al. [15] investigated the effect of the diameter of TiO_2 nanoparticles (10nm, 20nm, 30nm, and 50nm) on the thermal performance of the nanofluid in a tube heat exchanger. Elias et al. [16] studied the effect of shell and tube heat exchangers with different shapes and sphericity of nanoparticles on heat transfer flux. Xiao-Hui et al. [17] used the simulation to study the movement and suspension of the nanofluid in a heat exchanger system (HEs), and the results proved that the pulsatile flow and the optimum downhole structure could significantly enhance the thermal performance of the nanofluid. Finally, He et al. [18] reported that the dispersion of the TiO_2 nanoparticles into pure water improves the thermal conductivity of the nanofluids.

The presented literature survey shows that increasing nanoparticle concentration in nanofluids increases heat transfer efficiency. However, the amount of enhancement varies for different nanoparticles and their properties, including the solid volume fraction, the nanoparticle diameter, size, shape, and type. This study also provided experimental data on the effect of volume concentration on heat exchanger performance for various flows and Reynolds numbers. Therefore, the results of this study could be used to improve the heat exchangers in renewable energy systems (geothermal, solar energy, etc.) using Al_2O_3 nanofluids with different volume concentrations.

2 Experimental process

2.1 Description of experiment

The experimental system available at Boumerdes University, Algeria, is used to study the performance of a square shape heat exchanger operating with and without nanofluids. The schematic of the experimental setup is shown in Fig. 1. The system is composed of a Helicoidal Square Shape Heat Exchanger (HSSHE), a storage tank of water insolated by expanded polystyrene to minimize heat loss, a circulation pump, four valves, two plastic pipes, nine thermocouples, a 1200 W heater, cooling system, data logger, and a flow meter. The tube of HSSHE utilized in this experiment is made of copper, which has been extensively used in recent literature [19–21].

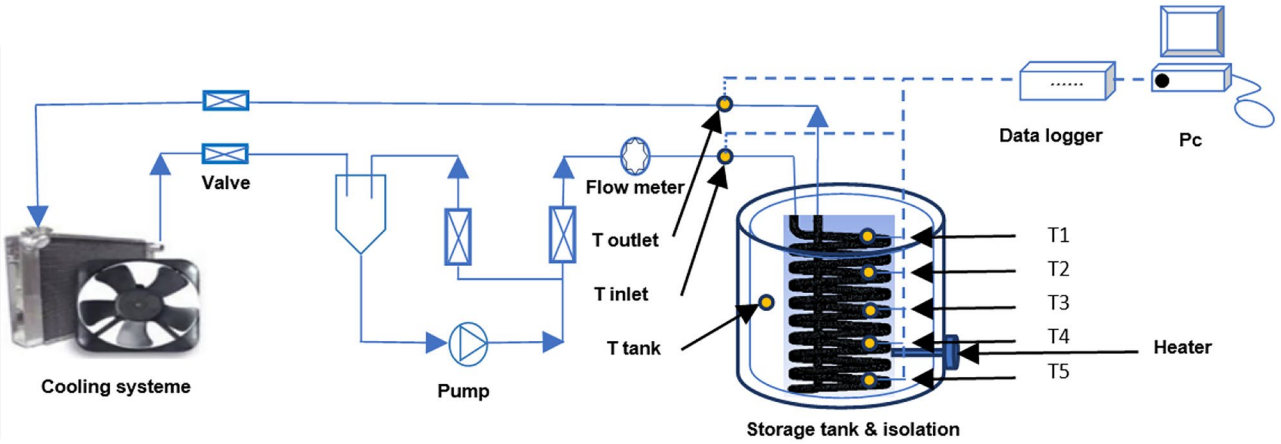

Fig. 1 Schematic diagram of the experimental setup and flow direction

The heat exchanger includes a copper square coiled tube, with the dimensions of the heat exchanger (HE) listed in Table 1 (case 1). An electrical heater (1200 W) is used to heat water around the heat exchanger and maintain the desired temperature adjusted by a thermostat during the experiment. The flow meter (SY 201 Type, Accuracy 1%) is installed and calibrated at three different flows (low, medium, and high). The cooling system maintains the ambient temperature. The K Type thermocouples are calibrated at different temperatures with GTH 1170 and are installed at various locations in the heat exchanger with an accuracy of (±0.3 C°). The centrifugal pump, which provides a flow range of 0-12 l/min, is installed to maintain liquid circulation in the cycle. After starting the pump, the flow rate is set to 2.4, 3, 3.7, and 4.3 l/min to generate flow Reynolds numbers of 4400, 5600, 6800, and 8000. Here Reynolds numbers were calculated based on the physical properties of the base fluid. For different nanoparticle concentrations in each test, the Reynolds number changes at the same flow rate since the effective viscosity of the nanofluid changes. However, the Reynolds number of the base fluid was used to compare different cases for a given flow rate. In addition, the range of nanoparticle concentrations used is low; therefore, the differences in Re are relatively small. All the sensors are connected to a personal PC to log and export the data. At the beginning of the operation process, we start with pure water, add the required nanoparticles to get the needed volume fraction, and use the zeta meter potential to test the stabilization of the liquid. Then, the same procedure is used for the two additional volume fractions.

Table 1 Dimensions of the helicoidal square shape heat exchanger (mm)

Parameter	Case 1	Case 2	Case 3
Total heights, b	224	264	304
Spacing, i	10	15	20

We conducted four sets of experiments using different liquids (nanofluids). The duration of each experiment is about three hours. The cases are:

Set 1: Used water.

Set 2: Used nanofluids with 0.1% volume fraction alumina nanoparticles.

Set 3: Used nanofluids with 0.25% volume fraction alumina nanoparticles.

Set 4: Used nanofluids with 0.5% volume fraction alumina nanoparticles.

It is observed that the heat exchanger passes through a transient state for a few minutes in the four sets of each flow, so all data exported from the transient period is discarded until it stabilizes and reaches a steady state.

Figure 2 shows the temperature variation over time when pure water is used in the fully developed region and after a transient period, allowing the accuracy of the thermocouples to be determined after the validation of measurements.

A helical square shape heat exchanger (HSSHE), as shown in Fig. 3, was used in the present study. The copper helical square coil tube has 14 and 16 mm inner and outer diameters, respectively. The single rib length is 12 cm, and the helicoidal square shape heat exchanger has 9 turns.

A three-dimensional computational model was developed, and the numerical simulations were performed using CFD to validate the experimental results. Figure 3 shows the model studied.

2.2 Computational mesh and grid independence study

The effective single-phase model is used to simulate the heat transfer performance of our prototype heat exchanger using the ANSYS Fluent, version 19.0 commercial software. A suitable computational mesh is needed to simulate the nanofluid flow and heat transfer accurately. Here a tetragonal element was used to obtain an appropriate mesh for the

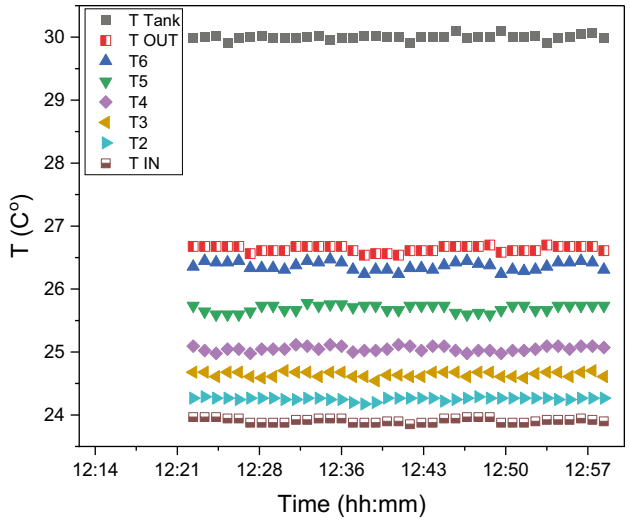

Fig. 2 Thermocouple's temperature accuracy & validation

complex geometry of the heat exchanger. Mesh convergence assessment was made depending on the error rate, which does not exceed 1 %. When the required convergence is reached, the number of nodes and elements is determined. The corresponding predicted average Nusselt numbers are shown in Fig. 4. This figure shows that a grid with 2,389,640 nodes provides grid-independent solutions. Therefore, this mesh was used in all subsequent simulation results, including those with various nanoparticle volumetric concentrations.

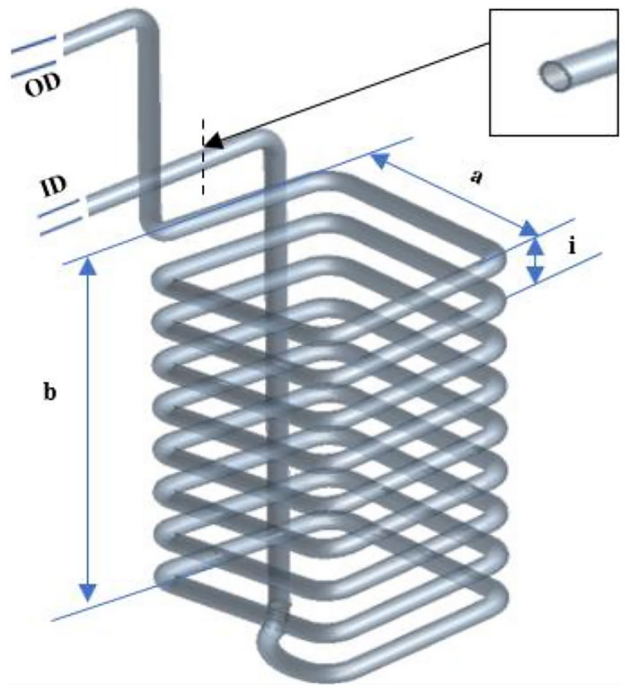

Fig. 3 3D model and dimensions of the heat exchanger studied

The 3D computational model was developed and used to study the nanofluid flow and heat transfer in the heat exchanger immersed in a water tank. The appropriate thermophysical properties of nanofluids were included in the computational model. It was assumed that the effect of gravity was negligible. In addition, the external pressure was assumed atmospheric, with a room temperature of 25 degrees. The dimension of the heat exchanger was 55cm ×18cm × 18 cm. More details of the mesh are shown in Fig. 5.

3 Nanofluids preparation

3.1 Preparation processes

The "two steps method" was used to disperse nano-powder into the base fluid. The Al_2O_3 particles with an average diameter of 50 nm were used in this experimental study to prepare nanofluids at different concentrations of 0.1%,0.25%, and 0.5%. A few drops of hydrochloric acid were added to the solution to assure stability by maintaining the value of PH away from the Iso Electric Point (IEP). For Al_2O_3, PH=9.4 leads to zero zeta potential [22]. The values of PH were recorded after using the electromagnetic agitator at 600 rpm for 90 min. In addition, an ultrasonic homogenizer was also used for 60 min. The PH was kept between 4.8 and 5.8, and the zeta potential value was up to 42 mV to ensure a homogeneous solution. All the experiments were conducted at ambient temperature. The electromagnetic mixing and ultrasonic steps were repeated after one day to maintain the stabilized homogeneous solution. After this procedure, no agglomeration was observed.

4 Thermo-physical nanofluid properties

For calculating the thermal conductivity of the nanofluid, we use the Maxwell equation, which is given as [23],

$$k_{nf} = k_{bf}\frac{k_p + 2k_{bf} - 2\left(k_{bf} - k_p\right)\varphi}{k_p + 2k_{bf} + \left(k_{bf} - k_p\right)\varphi} \tag{1}$$

Here k_p is the nanoparticle conductivity, and k_{bf} is the base fluid thermal conductivity. The volume fraction can be calculated from the weight concentration and is given as,

$$\varphi = \frac{\omega\rho_{bf}}{\omega\rho_{bf} + \rho_p(1-\omega)} \tag{2}$$

where ω is the weight concentration.

When the thermal conductivity of nanoparticles is more than that of liquid, for a small volume fraction φ, the nanofluid heat conductivity is given as,

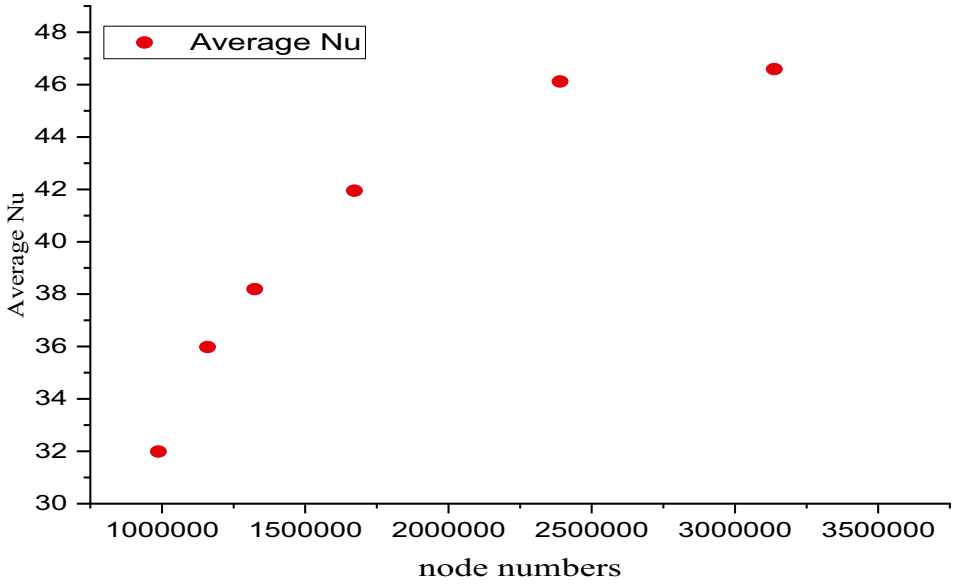

Fig. 4 Mesh independence study

$$k_{nf} = k_f(1 + 3\varphi) \tag{3}$$

This study assumes that nanoparticles are spherical and have a uniform size with a concentration < 1 %. The corresponding effective dynamic viscosity of nanofluids is given as [24],

$$\mu_{nf} = \mu_{bf}(1 + 7.3\varphi + 123\varphi^2) \tag{4}$$

The nanofluid density and the equivalent heat capacity are given, respectively, as,

$$\rho_{nf} = (1 - \varphi)\rho_{bf} + \varphi\rho_p \tag{5}$$

$$C_{p_{nf}} = \frac{(1 - \varphi)\left(\rho C_p\right)_{bf} + \varphi\left(\rho C_p\right)_p}{\rho_{nf}} \tag{6}$$

The variation of the thermophysical properties of nanofluid are listed in Table 2. It is seen that the viscosity of water/Al_2O_3 nanofluids increases by about 4% at the volume fraction of 0.5%.

5 Results and discussion

5.1 Validation

To validate the experimental study and estimate the accuracy, we measured the Nusselt number in the fully developed water turbulent flow region in a tube. In addition, we simulated the pure water flow condition in the same size tube and evaluated the corresponding Nusselt number (Nu). Finally, Nu values were also evaluated from the Dittus-Boelter correlation [26] given as

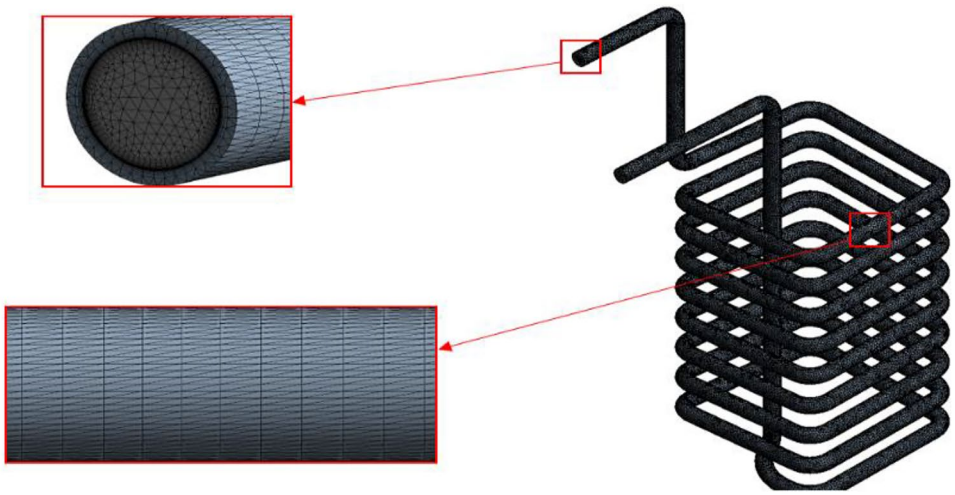

Fig. 5 The 3D geometry and the mesh used in the computational model

Table 2 Thermophysical properties for different nanofluids at various concentrations at T=298 K

liquids	Concentration (%)	K (W/m. K)	Cp (J/kg. K)	ρ (kg/m^3)	μ (kg/m. s)
Distilled water[25]	/	0.613	4179	997.1	0.001003
Water/Al_2O_3	0.1	0.618	4145.3	1004.5	0.001010
	0.25	0.622	4138.1	1012.4	0.001022
	0.5	0.631	4130.4	1027.9	0.001042

$$Nu = 0.023\, Re^{0.8} Pr^{n} \left(\begin{matrix} n = 0.4\, heating\ system \\ n = 0.3\, cooling\ system \end{matrix} \right) \tag{7}$$

Figure 6 compares the variation of the experimental Nu number of the pure water versus Re with the analytical correlation and the numerical simulation results. It is seen that the experimental data for the Nusselt number are in good agreement with the Dittus-Boelter correlation and the simulation results. Therefore, the experimental setup can be adapted to perform nanofluids-related tests.

In the subsequent sections, nanofluid heat transfer in the HSSHE for different solid concentrations is performed, and results are compared with pure water at various flow rates, $\dot{m}$, in the range of 2.4 to 4.3 L/m to determine the effect of nanoparticles on heat transfer. In these experiments, the heat transfer rate is evaluated by the following equation:

$$Q_{nf} = \dot{m} C_p (T_{out} - T_{in}) \tag{8}$$

The Nusselt number and heat transfer coefficient are calculated using,

$$Nu = \frac{h_{nf} D}{k_{nf}} \tag{9}$$

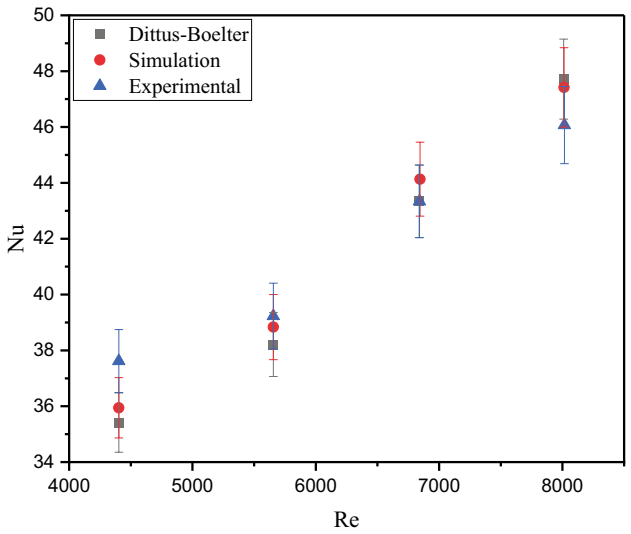

Fig. 6 Comparison of the experimental Nu data for the HSSHE versus Re with the analytical and simulation results

$$h_{nf} = \frac{Q_{nf}}{S\left(T_{w,ave} - T_{b,ave}\right)} \tag{10}$$

where $T_{w,ave}, T_{b,ave}$ are, respectively, the average temperature of the inner pipe surface and the average temperature of the fluid inside the pipe (bulk temperature), and S is the heated surface area.

5.2 Heat transfer flux exchange

Measuring the heat flux is necessary to calculate the heat transfer coefficient and the Nusselt number for the heat exchanger studied at different nanofluid concentrations. The fluid temperatures were measured at the inlet and outlet of the heat exchanger to determine the temperature difference, and various flow rates were used to study the Reynolds number on the heat flux.

Figure 7 shows the measured heat transfer rate for different aluminum oxide volume factions at different flow Reynolds numbers. Note that the Reynolds number is evaluated using the base fluid properties. In this study, the maximum particle concentration used is 0.5%, which according to Eq. (4) leads to an increase of 1.25% in viscosity that was neglected. Figure 8 displays the experimental heat exchange rate variations for different solid volume fractions versus flow rate. These figures show that the heat transfer rate increase with the volume fraction of aluminum oxide in the nanofluids. The increase in the Reynolds number also increases the heat transfer rate.

From the results of Figs. 7 and 8 indicate that nanofluid with the 0.5% aluminum oxide concentration has the highest heat transfer rate among the cases studied. For example, for a flow rate of 2.4 L/m and Re = 4400, the heat transfer rate is 556W, and at a flow rate of 4.3 L/m and Re= 8000, the heat transfer rate is 615W. This implies that the increase of the flow rate and Reynolds number also increases the heat exchange rate.

5.3 Heat transfer coefficient

Figure 9 presents the variation of heat transfer coefficient with Reynolds number at various nanofluid volume concentrations. It is seen that the heat transfer coefficient of the nanofluids for different concentrations is higher than the base fluid (pure water) and increases with the increase of the Reynolds number.

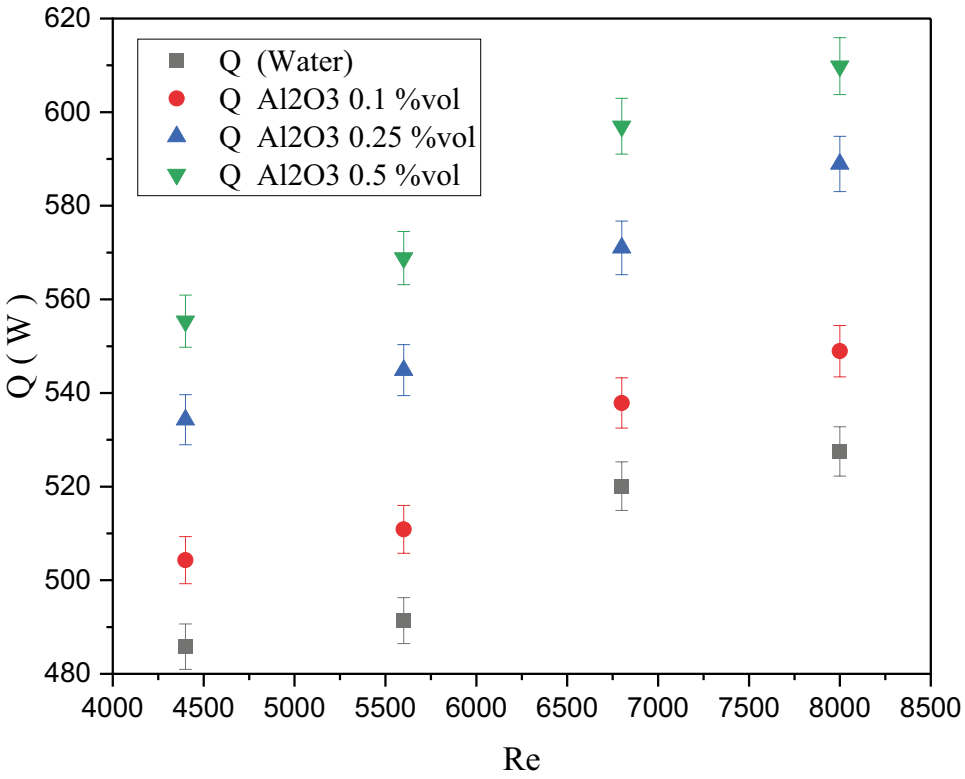

Fig. 7 Variation of experimental heat exchange rate for different solid volume fractions at various Re

Figure 9 shows a significant enhancement of the heat transfer coefficient (h) with an increase in particle concentration concentrations and an increase in flow Reynolds number. At the lowest Reynolds number of 4400, for a 0.1% nanoparticle concentration, the heat transfer coefficient increased by 5.37%. While at the 0.25% solid

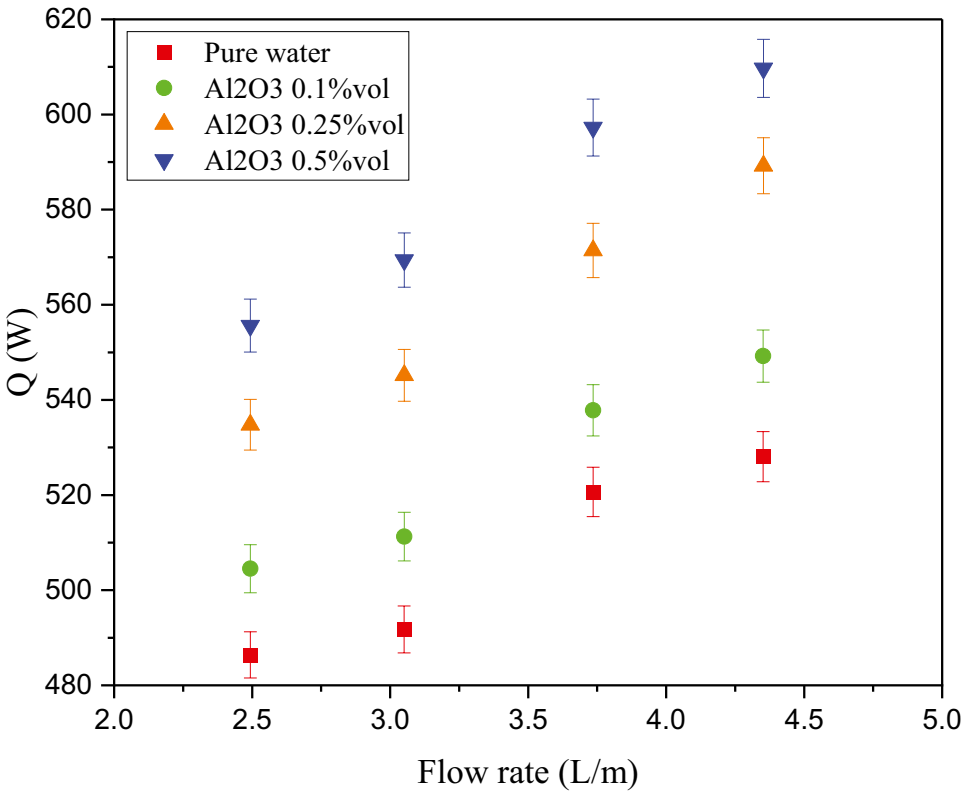

Fig. 8 Variations of experimental heat exchange rate for different solid volume fractions versus flow rate

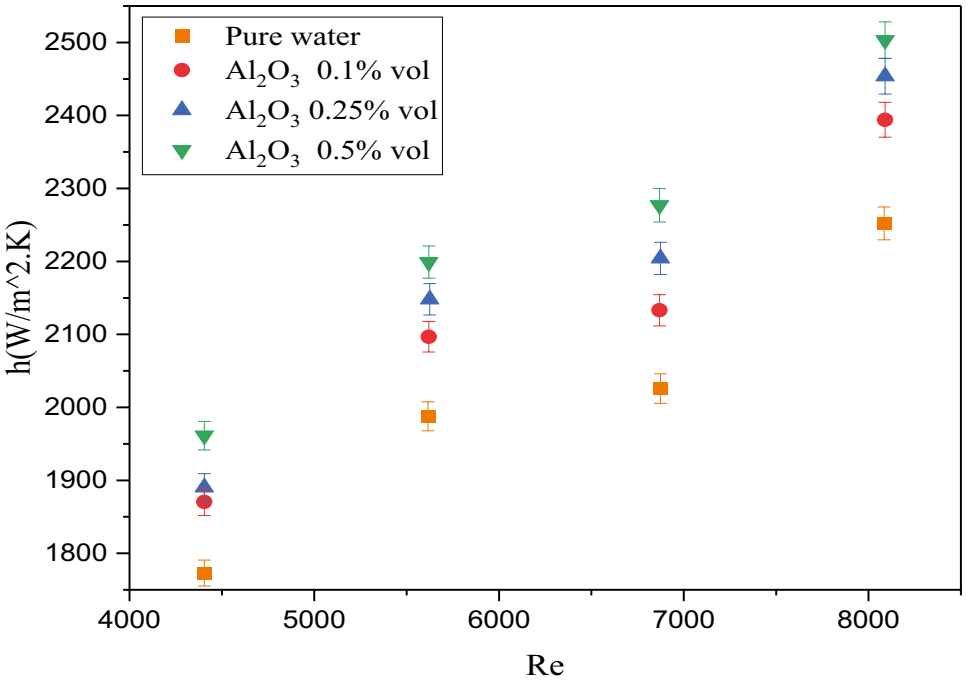

Fig. 9 Variations of the experimental heat transfer coefficient for the HSSHE versus Re for different nanoparticle concentrations

concentration, the heat transfer coefficient is increased by 6.29%, and at 0.5% concentration, the increase is about 9.64%. At the largest studied Reynolds number of 8000 with the same concentrations of 0.1%, 0.25%, and 0.5%, the heat transfer coefficient increases were 5.97%, 8.27%, and 10.10%, respectively. As noted before, the reason for the increase in the heat transfer coefficient of nanofluid compared with pure water is the addition of aluminum oxide nanoparticles to the water, which increases the effective heat conductivity of the fluid. The increase in the heat transfer rate with Re is due to the increase in convective transport.

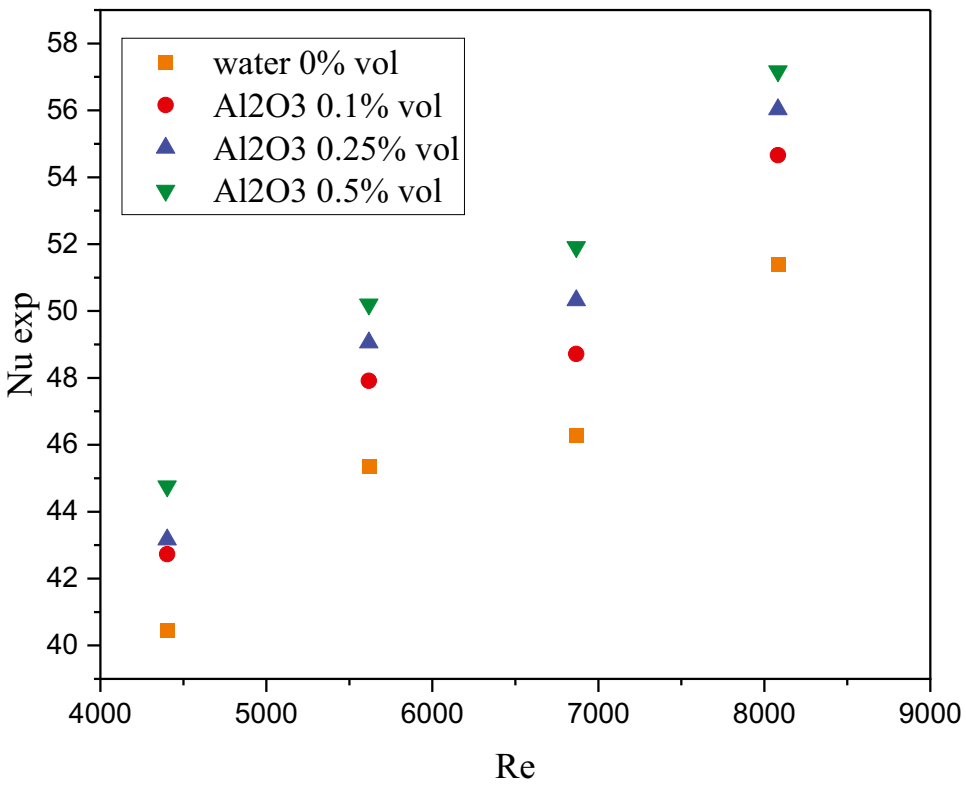

Fig. 10 Variations of the experimentally measured average Nusselt number with Re for different nanoparticle volume fractions

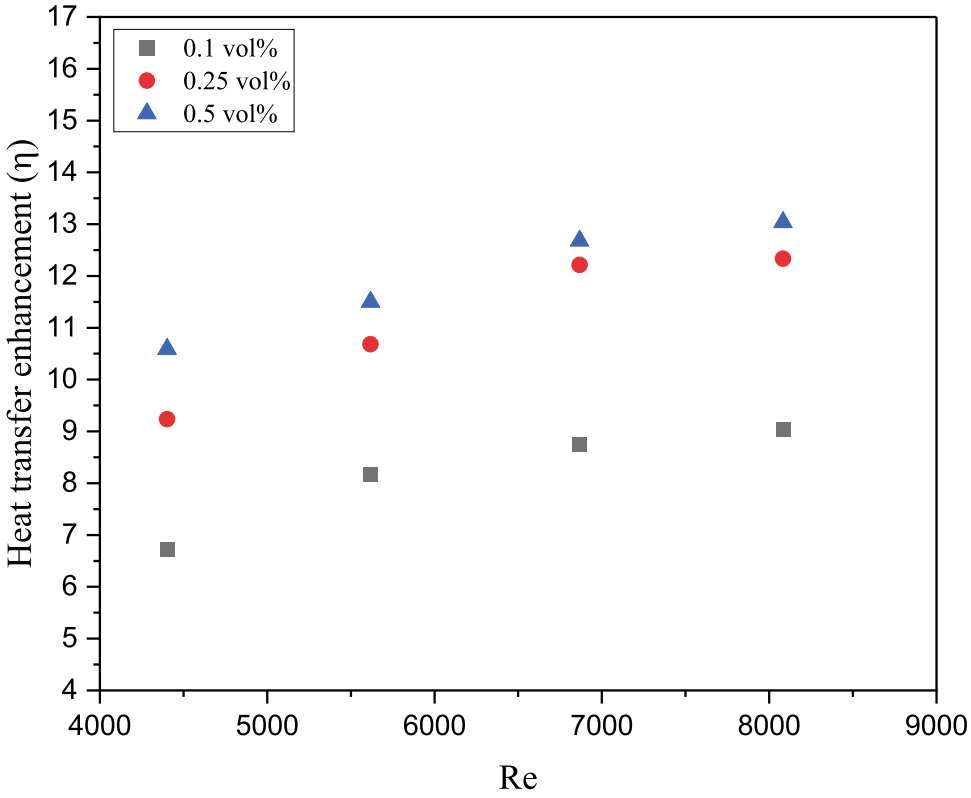

Fig. 11 Variations of heat enhancement versus Re for different nanoparticle volume fractions

5.4 Nusselt number calculation

Figure 10 shows the variations of the average Nusselt number of nanofluids and pure water versus Re. It is seen that the nanofluid Nusselt number is higher than that of pure water and increases by increasing the nanoparticle volume fraction and flow Reynolds number. In previous studies, it was suggested that the reason for augmentation in heat transfer

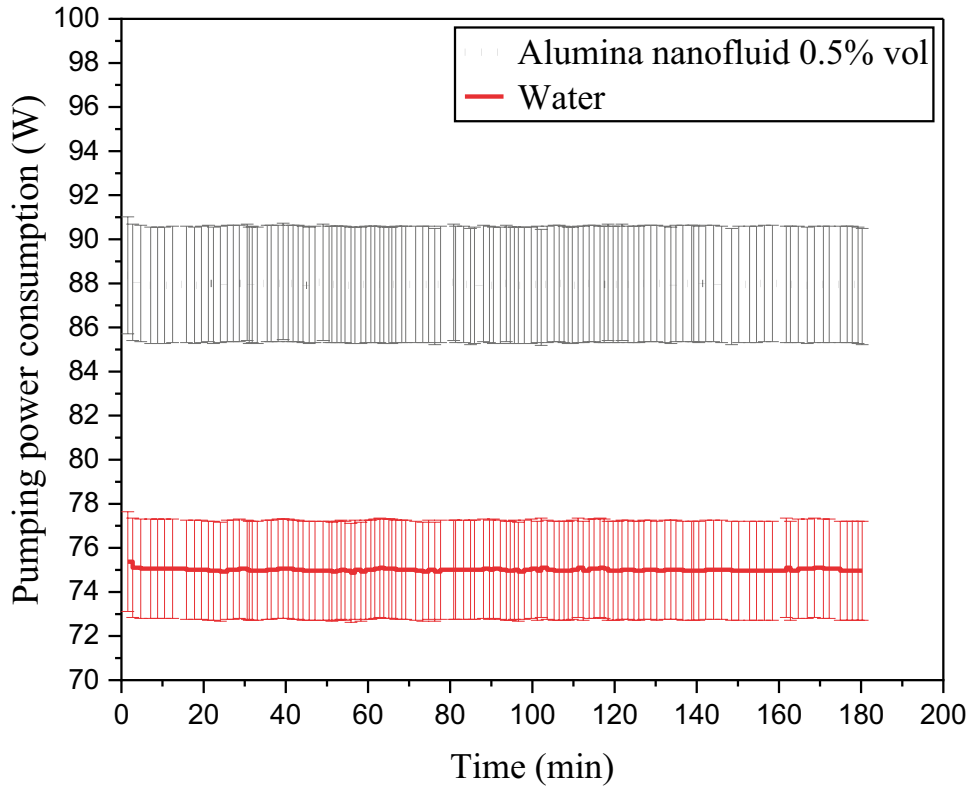

Fig. 12 Comparison of the pumping power consumptions of nanofluids with 0.5% solid fraction with water versus time.

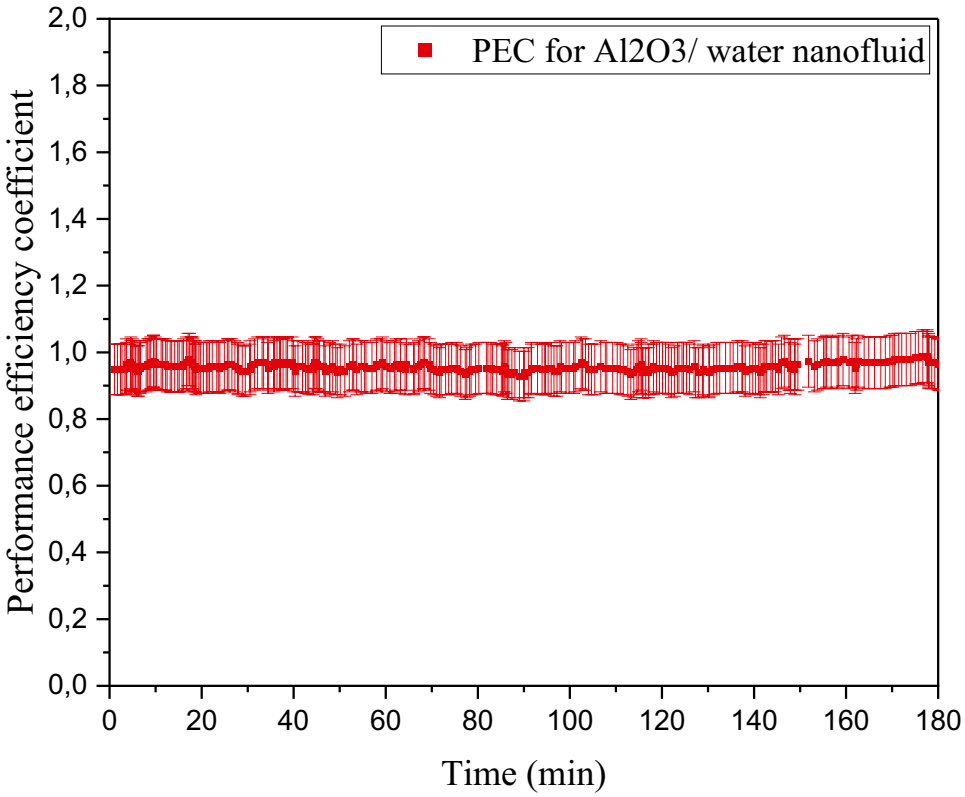

Fig. 13 Performance efficiency coefficient of Al_2O_3/water nanofluid at 0.5% concentration.

of the nanofluids is due to the Brownian motion of nanoparticles, migration of particles, and boundary layer thickness reduction [27, 28]. In addition, the shape of nanoparticles could also affect the heat transfer.

Figure 10 also shows that the Nusselt number (Nu) enhancement increases at higher values of the Reynolds number (Re) and the solid volume fraction. Generally, this improvement is due to the dispersion of nanoparticles into the base fluid, which increases effective thermal conductivity. The improvement of the Nusselt number with the increase in the Reynolds number is due to the convective transport and turbulence mixing.

6 Heat transfer enhancement

Heat transfer enhancement (η) is evaluated as a percentage increase of the Nusselt number of the nanofluid compared with the base fluid to study the efficiency of the heat exchanger and the effect of the nanofluid on heat transfer. Accordingly [29],

$$\eta = \left(\frac{Nu_{nf} - Nu_{bf}}{Nu_{nf}}\right) * 100\% \tag{12}$$

where Nu_{nf} and Nu_{bf} are the Nusselt numbers for the nanofluid and the base fluid, respectively.

Figure 11 illustrates the variation of heat transfer enhancement with the Reynolds numbers. The thermal performance of the heat exchanger increases when the Reynolds number increases. At the high Reynolds numbers, using nanofluids increases heat transfer enhancement. Using a nanofluid with a high concentration leads to high thermal performance at different Reynolds numbers. Over the studied range of Reynolds numbers and the concentrations, the largest increase in the thermal performance factor was 13% at the Re=8000, and the volume fraction was 0.5%.

6.1 Pumping power

This section concerns the heat exchanger system's energy efficiency and pumping power needs when nanofluids are used. The effectiveness of heat transfer fluids Eq. (13) could be measured on the ratio of the heat transfer rate given by Eq. (8) to the amount of pumping energy consumption [30],

$$\eta_{e,bf} = \frac{Q_{bf}}{W_{p_{bf}}} \tag{13}$$

We can applicate the same ratio for the nanofluid:

$$\eta_{e,nf} = \frac{Q_{nf}}{W_{p_{nf}}} \tag{14}$$

Figure 12 compares the measured pumping powers of nanofluids with 0.5% solid fraction with pure water. It is seen that the pumping power consumption of pure water in the range of 75 watts, while the power consumption of nanofluids with 0.5% aluminum oxide particle is in the range of 88 watts. Therefore, using nanofluids at a concentration of 0.5% requires 14.77 % more pumping power than pure water.

The performance efficiency coefficient (PEC) is used to compare the energy efficiency of the nanofluid and water as shown in Fig. 13. Therefore, the final PEC of the system is given as [31],

$$PEC = \frac{\eta_{e,nf}}{\eta_{e,bf}} \tag{15}$$

where W_p is the pumping power consumption, $\eta_{e,nf}, \eta_{e,bf}$ are the effectiveness of heat transfer of nanofluids and base fluids, respectively.

7 Conclusions

We presented an experimental study using nanofluids with different concentrations in a novel helical shape heat exchanger. The heat transfer coefficient and Nusselt number of nanofluid with different concentrations were measured versus Reynolds numbers and various flow rates up to 4.3 L/m. The efficiency of the heat exchanger was also investigated to assess the effect of using nanofluid on the heat transfer of the system. The presented results showed that using nanofluids increased the heat transfer performance compared to a pure liquid.

The main findings are:

1. The heat transfer flux increased by 13.46% for the nanofluid with a concentration of 5% and a flow rate of 4.3 L/m. Therefore, the heat exchanger heat transfer was enhanced by changing the working fluid from water to nanofluids.
2. The Nusselt number increased by 10.43%, and the heat transfer coefficient by 9.64% for nanofluid with a volume concentration of 5% and Re = 8000.
3. The heat exchange performance increased as the concentration of nanofluid or flow Reynolds number increased.

Computational modeling of flow and heat transfer of aluminum oxide nanofluid in the helical heat exchanger is left for a future study.

References

1. Saedodin S, Zaboli M, Rostamian SH (2020) Effect of twisted turbulator and various metal oxide nanofluids on the thermal performance of a straight tube: Numerical study based on experimental data. Chem Eng Processing-Process Intens 158
2. Singh S, Negi JS, Bisht S, Sah H (2019) Thermal performance and frictional losses study of solid hollow circular disc with rectangular wings in circular tube. Heat Mass Transf 55(10):2975–2986
3. Keklikcioglu O, Ozceyhan V (2017) Entropy generation analysis for a circular tube with equilateral triangle cross sectioned coiled-wire inserts. Energy 139:65–75
4. He Y, Liu L, Li P, Ma L (2018) Experimental study on heat transfer enhancement characteristics of tube with cross hollow twisted tape inserts. Appl Therm Eng 131:743–749
5. Ibrahim MM, Essa MA, Mostafa NH (2019) A computational study of heat transfer analysis for a circular tube with conical ring turbulators. Int J Therm Sci 137:138–160
6. Zheng N, Liu P, Wang X, Shan F, Liu Z, Liu W (2017) Numerical simulation and optimization of heat transfer enhancement in a heat exchanger tube fitted with vortex rod inserts. Appl Therm Eng 123:471–484
7. Faizal M, Bouazza A, Singh RM (2016) Heat transfer enhancement of geothermal energy piles. Renewable Sustain Energ Rev 57:16–33
8. Boughanmi H, Lazaar M, Bouadila S, Farhat A (2015) Thermal performance of a conic basket heat exchanger coupled to a geothermal heat pump for greenhouse cooling under Tunisian climate. Energy Build 104:87–96
9. Kumar V, Tiwari AK, Ghosh SK (2015) Application of nanofluids in plate heat exchanger: a review. Energy Conv Manag 105:1017–1036
10. Nasir FM, Mohamad AY (2006) Heat transfer of CuO-water based nanofluids in a compact heat exchanger. ARPN J Eng Appl Sci 11(4):2517–2523
11. Wilk J, Smusz R, Grosicki S (2017) Thermophysical properties of water based Cu nanofluid used in special type of coil heat exchanger. Appl Therm Eng 127:933–943
12. Karuppasamy M, Saravanan R, Chandrasekaran M, Muthuraman V (2020) Numerical exploration of heat transfer in a heat exchanger tube with cone shape inserts and Al2O3 and CuO nanofluids. Maters Today: Proc 21:940–947
13. Narei H, Ghasempour R, Noorollahi Y (2016) The effect of employing nanofluid on reducing the bore length of a vertical ground-source heat pump. Energ Conversion 123:581–591
14. Jamshidi N, Mosaffa A (2018) Investigating the effects of geometric parameters on finned conical helical geothermal heat exchanger and its energy extraction capability. Geothermics 76:177–189
15. Arani AA, Amani J (2013) Experimental investigation of diameter effect on heat transfer performance and pressure drop of TiO2–water nanofluid. Exp Thermal Fluid Sci 44:520–533
16. Elias M et al (2013) Effect of nanoparticle shape on the heat transfer and thermodynamic performance of a shell and tube heat exchanger. Int Comm Heat Mass Transf 44:93–99
17. Sun X-H, Yan H, Massoudi M, Chen Z-H, Wu W-T (2018) Numerical simulation of nanofluid suspensions in a geothermal heat exchanger. Energies 11(4):919
18. He Y, Jin Y, Chen H, Ding Y, Cang D, Lu H (2007) Heat transfer and flow behaviour of aqueous suspensions of TiO2 nanoparticles (nanofluids) flowing upward through a vertical pipe. Int J Heat Mass Transf 50(11–12):2272–2281
19. Cimmino M, Bernier M (2015) Experimental determination of the g-functions of a small-scale geothermal borehole. Geothermics 56:60–71
20. Yang W, Zhang S, Chen Y (2014) A dynamic simulation method of ground coupled heat pump system based on borehole heat exchange effectiveness. Energ Buildings 77:17–27
21. Li W, Li X, Peng Y, Wang Y, Tu J (2018) Experimental and numerical investigations on heat transfer in stratified subsurface materials. Appl Therm Eng 135:228–237

22. Allouni ZE, Cimpan MR, Høl PJ, Skodvin TG (2009) Nils R "Agglomeration and sedimentation of TiO2 nanoparticles in cell culture medium," Colloids surfaces B: Biointerfaces 68(1):83–87
23. Hamilton RL, Crosser O (1962) Thermal conductivity of heterogeneous two-component systems. Industrial Eng Chem Fundamentals 1(3):187–191
24. El Bécaye Maïga Set al (2006) Heat transfer enhancement in turbulent tube flow using Al2O3 nanoparticle suspension. 16(3):275–292
25. El Bécaye Maïga S, Tam Nguyen C, Galanis N, Roy G, Maré T, Coqueux M (2006) Heat transfer enhancement in turbulent tube flow using Al2O3 nanoparticle suspension. Int J Numerical Methods Heat Fluid Flow
26. Dittus F, Boelter L (1985) Heat transfer in automobile radiators of the tubular type. Int Comm Heat Mass Transf 12(1):3–22
27. Kim Det al (2009) Convective heat transfer characteristics of nanofluids under laminar and turbulent flow conditions,. 9(2): e119–e123
28. Duangthongsuk W, Wongwises S (2010) An experimental study on the heat transfer performance and pressure drop of TiO2-water nanofluids flowing under a turbulent flow regime. 53(1–3):334–344
29. Togun Het al (2015)Thermal performance of nanofluid in ducts with double forward-facing steps. 47:28–42
30. Du R, Jiang D, Wang Y, Shah KW (2020) An experimental investigation of CuO/water nanofluid heat transfer in geothermal heat exchanger. 227:110402.
31. Kong M, Alvarado JL, Thies C, Morefield S, Marsh CP (2017) Field evaluation of microencapsulated phase change material slurry in ground source heat pump systems. 122:691–700